

All-order relativistic many-body theory of low-energy electron-atom scattering

Yongjun Cheng,^{1,2,*} Li Yan Tang,^{2,3,†} J. Mitroy,^{2,‡} and M. S. Safronova^{4,§}

¹Center for Theoretical Atomic and Molecular Physics, The Academy of Fundamental and Interdisciplinary Science, Harbin Institute of Technology, Harbin 150080, People's Republic of China

²Centre for Antimatter-Matter Studies and School of Engineering, Charles Darwin University, Darwin, Northern Territory 0909, Australia

³State Key Laboratory of Magnetic Resonance and Atomic and Molecular Physics, Wuhan Institute of Physics and Mathematics, Chinese Academy of Sciences, Wuhan 430071, People's Republic of China

⁴Department of Physics and Astronomy, University of Delaware, Newark, Delaware 19716, USA

(Received 31 October 2013; published 8 January 2014)

A generalization of the box-variational method is developed to describe particle scattering with the Dirac equation. The method is applied to extract phase shifts from all-order single + double relativistic many-body perturbation theory calculations of the electron-helium, electron-neon, and electron-krypton systems. Comparisons with experimental elastic and momentum transfer cross sections are made. Agreement at the 1% to 2% level is achieved for helium and neon. The scattering length for krypton is 4% smaller in magnitude than experimental estimates derived from swarm experiments.

DOI: [10.1103/PhysRevA.89.012701](https://doi.org/10.1103/PhysRevA.89.012701)

PACS number(s): 34.80.Bm, 34.10.+x, 03.65.Nk

I. INTRODUCTION

The box-variational method [1,2] is a very simple method for solving the Schrödinger equation for scattering systems. In this approach, the system is placed in an infinite wall cavity of radius R and the wave function will satisfy the conditions $\psi(0) = \psi(R) = 0$. The energies in the cavity E_n for s -wave scattering can be used to determine the phase shifts δ through the relation $\sin(k_n R + \delta_n) = 0$, where $k_n = \sqrt{2E_n}$. This leads to the identity $\delta_n = n\pi - R\sqrt{2E_n}$. This approach can be generalized to higher ℓ partial waves with the general boundary condition $j_\ell(k_n R) - \tan(\delta_n)n_\ell(k_n R) = 0$, where j_ℓ and n_ℓ are spherical Bessel functions. The box-variational method has been applied intermittently to solve the continuum Schrödinger equation in a variety of contexts [3–8].

The increasing usage of B -spline methods as a numerical workhorse for solving the Schrödinger and Dirac equations in atomic physics [9–12] is interesting since B -spline boundary conditions are compatible with the application of the box-variational method. In this manuscript the ideas of the box-variational method are applied to the description of low-energy electron-atom scattering using the all-order single-double implementation of relativistic many-body perturbation theory (MBPT) [13,14]. In this method, all possible single and double excitations from the Dirac-Fock (DF) wave function are iterated to all orders of perturbation theory. Triple excitations are included perturbatively. The radial parts of the single electron states used in the calculation are represented by a B -spline basis that is effectively complete. This gives a model of electron-atom scattering that is underpinned by state of the art atomic structure theory.

The major difference from previous applications of the box variational method lies in the specification of the boundary conditions. The natural boundary condition to choose for the

Schrödinger equation is the condition $\psi(R) = 0$. However, this boundary condition is not widely used for the Dirac equation. Instead, one typically uses the boundary conditions of the MIT bag model [9,15] which result in the large, $P(r)$, and small, $Q(r)$, components being set equal at the boundary, i.e., $P(R) = Q(R)$.

In this paper, detailed results for low-energy electron scattering from three atoms, namely, helium, neon, and krypton are presented. The calculations for helium were done as a validation of the method while those on neon are in excellent agreement with existing experimental cross sections. The MBPT calculation underestimates experimental values of the scattering length for krypton, obtained from swarm experiments, by about 4%.

II. FORMALISM

A. Box calculations

The MIT–Notre Dame boundary conditions impose the condition $P(R) = Q(R)$. The conditions are applied to the asymptotic form of the scattering wave functions. These are written in the relativistic case [16] as

$$P(r) = krj_\ell(kr) - \tan(\delta)krn_\ell(kr) \quad (1)$$

and

$$Q(r) = \frac{ck[krj_{\ell-1}(kr) - \tan(\delta)krn_{\ell-1}(kr)]}{E + 2m_e c^2}, \quad \kappa = \ell, \\ = -\frac{ck[krj_{\ell+1}(kr) - \tan(\delta)krn_{\ell+1}(kr)]}{E + 2m_e c^2}, \quad (2)$$

$$\kappa = -\ell - 1,$$

where j_ℓ and n_ℓ are spherical Bessel functions of the first and second kind and where the total energy and wave number k are related by

$$(E + m_e c^2)^2 = p^2 c^2 + m_e^2 c^4, \quad (3)$$

$$k = p = \sqrt{E(E + 2m_e c^2)}/c.$$

*cyj83mail@gmail.com

†lytang@wipm.ac.cn

‡jxm107@rsphysse.anu.edu.au

§msafrono@udel.edu

Applying the boundary conditions to a state with energy E in a cavity of radius R leads to the relations

$$\begin{aligned} krj_\ell(kR) - \tan(\delta)krn_\ell(kR) \\ = \frac{-kc[kRj_{\ell-1}(kR) - \tan(\delta)kRn_{\ell-1}(kR)]}{E + 2m_e c^2}, \quad \kappa > 0, \\ = \frac{kc[Rrj_{\ell+1}(kR) - \tan(\delta)kRn_{\ell+1}(kR)]}{E + 2m_e c^2}, \quad \kappa < 0. \end{aligned} \quad (4)$$

Expressions for the tangent of the phase shift can then be written as

$$\begin{aligned} \tan(\delta) &= \frac{-kcj_{\ell-1}(kR) - (E + 2m_e c^2)j_\ell(kR)}{-kcn_{\ell-1}(kR) - (E + 2m_e c^2)n_\ell(kR)}, \quad \kappa > 0, \\ &= \frac{-kcj_{\ell+1}(kR) + (E + 2m_e c^2)j_\ell(kR)}{-kcn_{\ell+1}(kR) + (E + 2m_e c^2)n_\ell(kR)}, \quad \kappa < 0. \end{aligned} \quad (5)$$

Application of these results only gives the phase shift at the cavity radius R . A correction was added to this phase shift to estimate the $r \rightarrow \infty$ phase shift. This correction was determined by integrating the Dirac equation from $r = R$ to $r = 10R$ in a $-\alpha_d/(2r^4)$ potential field, where α_d is the static dipole polarizability [17]. The correction was typically very small, only altering the phase shift in the fifth significant digit.

B. The all-order many-body calculations

The energies of the electron + atom system were evaluated using the single-double all-order version of relativistic MBPT [13,14,18]. In this linearized coupled-cluster approach, all the single and double (SD) excitations from the Dirac-Fock (DF) wave function are iterated to all orders of perturbation theory. The MBPT-SD wave function $|\Psi_v\rangle$ of the electron state v is represented by the expansion

$$\begin{aligned} |\Psi_v\rangle = & \left[1 + \sum_{ma} \rho_{ma} a_m^\dagger a_a + \frac{1}{2} \sum_{mnab} \rho_{mnab} a_m^\dagger a_n^\dagger a_b a_a \right. \\ & \left. + \sum_{m \neq v} \rho_{mv} a_m^\dagger a_v + \sum_{mna} \rho_{mnva} a_m^\dagger a_n^\dagger a_a a_v \right] |\Psi_v^{(0)}\rangle, \end{aligned} \quad (6)$$

where $|\Psi_v^{(0)}\rangle$ is the lowest-order atomic state vector. The quantities ρ_{ma} and ρ_{mv} are single-excitation coefficients for the core and ‘‘valence’’ electrons and ρ_{mnab} and ρ_{mnva} are double-excitation coefficients for the core and valence electrons, respectively; the indices m and n range over all possible virtual states while the indices a and b range over all occupied core states. The valence electron in this case is the scattering electron. The equations for the correlation energy and the excitation coefficients are solved iteratively for each electron state needed for the current project, which is equivalent to summing dominant many-body perturbation terms to all orders. To ensure high numerical stability of the data for different states, the iteration process was continued until the relative change in the valence energy was less than 10^{-8} .

This method was originally developed for the calculation of the properties of alkali-metal atoms and other similar systems with one valence electron. In the current implementation, the single-particle wave functions are constructed for the

corresponding noble-gas atom. The radial parts of the single-particle wave functions are expanded in terms of a large B -spline basis and for all practical purposes this basis constituted a complete set. Large basis sets are needed to ensure high numerical accuracy. The size of the B -spline basis depended on the cavity radius, with basis dimensions ranging from 50 to 100. The order of the B -spline basis was $k = 13$. All all-order calculations were carried out with $L_{\max} = 6$ partial waves. To evaluate the contribution of the higher partial waves, second-order energy calculations were carried out with $L_{\max} = 6$ and $L_{\max} = 10$ partial waves. The difference was added to all final values. The size of the contribution from $L > 10$ partial waves was estimated by extrapolating second-order results and was found to be negligible.

We used two approaches that allowed us to incorporate important triple excitations into the calculations. First, we added the terms resulting from the triple excitations that appear in the third-order perturbation theory. Such terms are calculated using separated third-order energy code and are added to the MBPT-SD results, the corresponding values are labeled SD_{extra}. In a second, more sophisticated approach [14], the valence triple-excitation term

$$\frac{1}{6} \sum_{mnrab} \rho_{mnrwab} a_m^\dagger a_n^\dagger a_r^\dagger a_b a_a a_v |\Psi_v^{(0)}\rangle \quad (7)$$

is added to the expansion (6). Then the correlation energy and single-excitation ρ_{mv} equations are modified perturbatively to account for certain classes of triple excitations. This procedure makes the SD energy complete in the third order and also includes triple-excitation terms appearing in the fourth and higher orders. This approach with its perturbative treatment of triple excitations is termed the MBPT-SDpT method.

C. Interpolation of the phase shifts

Application of the box conditions only gives the phase shifts at certain discrete energies in the continuum. The desired outcome of any scattering calculation should be the determination of the phase shifts and the cross sections at any energy. The approach adopted was to simply develop interpolating functions that can give the phase shifts at any energy of interest.

The phase shifts themselves are not directly interpolated. Rather the function used for the interpolations incorporates information on the expected variation of the phase shifts using modified effective range theory (MERT) [19–21]. This approach has previously been utilized when creating an interpolating function to give a usable representation of high precision Kohn variational calculations of electron-helium scattering [22,23].

As an example, consider the s -wave phase shift. A MERT expansion for this phase shift can be written as

$$\tan(\delta) = -A_{\text{scat}} k \left(1 + \frac{4}{3} \alpha_d k^2 \ln(k/D) \right) + \frac{\pi}{3} \alpha_d k^2 - Ek^4, \quad (8)$$

where A_{scat} is the scattering length. Upon rearrangement, one can define the function

$$w(k, \delta) = -\frac{\tan(\delta) - Ek^4 + \frac{\pi}{3} \alpha_d k^2}{k \left[1 + \frac{4}{3} \alpha_d k^2 \ln(k/D) \right]}. \quad (9)$$

TABLE I. Interpolating functions $w(\delta, k)$ for the phase shifts for each L value. Here α_d gives the dipole polarizability. The w_0 column gives the value of $w(\delta, k)$ for the SDpT calculation in the $k = 0$ limit. The p -wave interpolating function for krypton is defined differently for $j = 1/2$ and $j = 3/2$.

L	$w(\delta, k)$	w_0	D	E
e^- -He $\alpha_d = 1.383\,760\,79$ a.u.				
0	$\frac{\tan(\delta) - Ek^4 + \frac{\pi}{3}\alpha_d k^2}{k \left[1 + \frac{4}{3}\alpha_d k^2 \ln(k/D)\right]}$	1.189	0.780	0.400
1	$\frac{\arctan\left(\frac{\pi}{15}\alpha_d k^2\right) - \delta}{k^3}$	0.039		
2	$\frac{\tan(\delta)}{k^2}$	0.0402		
e^- -Ne $\alpha_d = 2.670$ a.u.				
0	$\frac{\tan(\delta) - Ek^4 + \frac{\pi}{3}\alpha_d k^2}{k \left[1 + \frac{4}{3}\alpha_d k^2 \ln(k/D)\right]}$	0.224	5.0	-2.8
1	$\frac{\arctan\left(\frac{\pi}{15}\alpha_d k^2\right) - \delta}{k^3}$	2.55		
2	$\frac{\tan(\delta)}{k^2}$	0.0752		
e^- -Kr $\alpha_d = 16.766$ a.u.				
0	$\frac{\tan(\delta) - Ek^4 + \frac{\pi}{3}\alpha_d k^2}{k \left[1 + \frac{4}{3}\alpha_d k^2 \ln(k/D)\right]}$	-3.23	0.122	-15.0
1 ($j = 1/2$)	$\frac{\arctan\left(\frac{\pi}{15}\alpha_d k^2\right) - \delta}{k^3}$	17.6		
1 ($j = 3/2$)	$\frac{\arctan\left(\frac{\pi}{15}\alpha_d k^2\right) - \delta}{k^3}$	18.4		
2	$\frac{\arctan\left(\frac{\pi}{105}\alpha_d k^2\right) - \delta}{k^3}$	0.600		
3	$\frac{\tan(\delta)}{k^2}$	0.156		

This function varies less rapidly with k than the phase shift and therefore is easier to interpolate. The interpolation was done using natural cubic splines. The values of D and E are chosen manually to make $w(k, \delta)$ roughly constant at the smallest values of k . The phase shift can then be easily computed at any k once a representation of $w(k, \delta)$ has been constructed. A complete representation of the phase shift at all k depends weakly on an estimate of the limiting form of the phase shift as $k \rightarrow 0$. The limiting value of $w(k, \delta)$ at $k = 0$ could be estimated to a precision of better than 0.5% by examination of $w(k, \delta)$ for the smallest values of k .

Table I gives details of the functions used to create continuous functions of the phase shift as a function of energy. These functions are reliant on values of the dipole polarizability which were sourced from Ref. [17]. There were no obvious problems arising from the use of interpolation and the behavior of the interpolated phase shifts as a function of energy was typically very smooth.

D. Cross sections

The total elastic, σ_T , and momentum transfer, σ_{MT} , cross sections are calculated using formulas from Ref. [24],

namely,

$$\sigma_T = \frac{4\pi}{k^2} \sum_{\ell=0} [(\ell+1) \sin^2(\delta_\ell^+) + \ell \sin^2(\delta_\ell^-)], \quad (10)$$

$$\sigma_{MT} = \frac{4\pi}{k^2} \sum_{\ell=0} \left(\frac{(\ell+1)(\ell+2)}{(2\ell+3)} \sin^2(\delta_\ell^+ - \delta_{\ell+1}^+) + \frac{\ell(\ell+1)}{(2\ell+1)} \sin^2(\delta_\ell^- - \delta_{\ell+1}^-) + \frac{(\ell+1)}{(2\ell+1)(2\ell+3)} \sin^2(\delta_\ell^+ - \delta_{\ell+1}^-) \right). \quad (11)$$

In these equations, δ_ℓ^+ refers to the phase shift with $j = \ell + \frac{1}{2}$ and δ_ℓ^- refers to the phase shift with $j = \ell - \frac{1}{2}$.

The low- ℓ phase shifts were obtained by explicit MBPT-SDpT calculations. Higher- ℓ phase shifts are given by the MERT formula [19–21]:

$$\tan(\delta_\ell) = \frac{\pi \alpha_d k^2}{(2\ell-1)(2\ell+1)(2\ell+3)}. \quad (12)$$

III. HELIUM

The first calculation performed was a test calculation on the electron-helium system. Previous calculations include those using the R -matrix [25], multiconfiguration Hartree-Fock (MCHF) [26] and Kohn-variational approaches [22]. The Kohn variational (KV) calculations of Nesbet have been accepted as giving a benchmark set of theoretical phase shifts that are compatible with experimental data [27,28].

There have been numerous experiments on the electron-helium system at energies below the first excitation threshold. Most of the experimental elastic cross-section data referenced in the present manuscript are taken from transmission experiments which measure the attenuation of an electron beam as it passes through a gas cell [29–31]. Electron swarm experiments that measure the drift velocity generate a momentum transfer cross section by an analysis involving the solution of the Boltzmann equation [32,33].

The MBPT-SDpT calculations were performed in a cavity of radius $32.741\,081\,a_0$. The long-range correction to the phase shift made by integrating the $-\alpha_d/(2r^4)$ polarization potential outwards from R was always less than 0.0001 rad with the correction being largest at the smallest energies.

Figure 1 plots δ/k vs k for the s -wave phase-shift and compares the results with the KV phase shifts [22]. The KV phase shift curve was computed from the spline function presented in Ref. [22] which was based on the explicitly calculated KV phase shifts given at intervals of $0.10\,a_0^{-1}$. The s -wave phase shifts are also detailed at momentum intervals of $0.10\,a_0^{-1}$ in Table II. For all practical purposes, the s -wave MBPT-SDpT phase shifts are identical with the KV phase shifts, with the one exception occurring at $k = 0.30\,a_0^{-1}$, where the KV phase shift is 0.0015 rad different from the SDpT phase shift. The KV phase shift shown in Fig. 1 appears to have an irregularity at $k = 0.30\,a_0^{-1}$. This irregularity is also evident in the coefficients of the spline representation used to construct a continuous presentation of the KV phase shift [22]. There is another irregularity in the KV phase shift at $k = 0.60\,a_0^{-1}$.

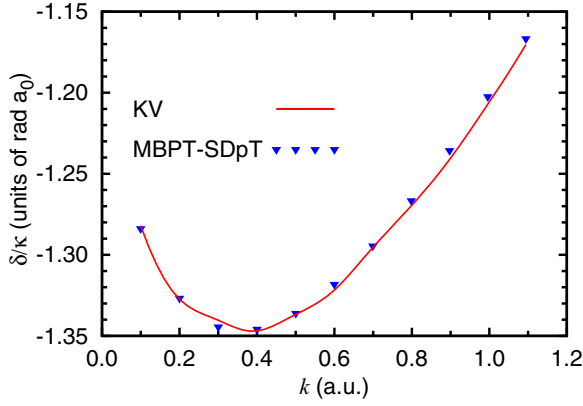


FIG. 1. (Color online) The ratio of the s -wave phase shift (in units of rad) divided by k (in units of a_0^{-1}) for e^- -He scattering. Phase shifts from a KV calculation [22] are also shown.

But, taken as a whole, the comparisons for the s -wave helium phase shift validate the methodology used to extract the phase shifts from the MBPT energies.

The low-energy s , p , and d wave shifts are presented in Table II. The SDpT calculations actually give slightly different phase shifts for the two different members of the spin-orbit doublet. However, the largest difference between the $p_{1/2}$ and $p_{3/2}$ phase shifts was only 0.00002 rad. So the approach adopted here was to simply average the phase shifts of the spin-orbit doublets. The MBPT-SDpT p -wave phase shifts are about 1%–4% smaller than the KV phase shifts, with the differences being largest at the lowest energies. These minor differences in the p -wave phase shifts have minimal impact on the cross section. The elastic cross section is dominated by s -wave scattering and even at $k = 1.0 a_0^{-1}$ the s -wave cross section makes up 85% of the cross section. The SDpT phase shifts are tabulated on a momentum grid with a spacing of $0.01 a_0^{-1}$ in the Supplemental Material [34].

The momentum transfer cross section σ_{MT} for helium is plotted in Fig. 2. The experimental momentum transfer cross

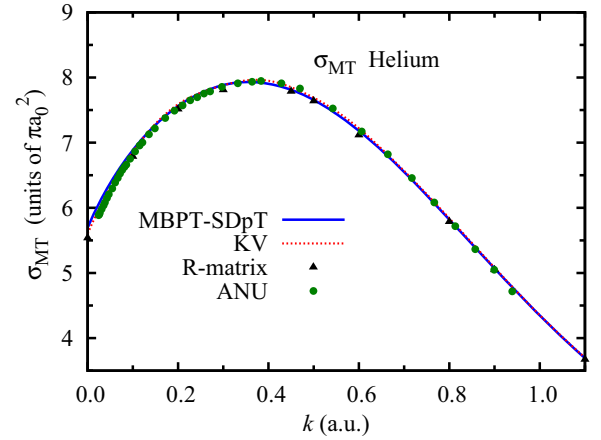


FIG. 2. (Color online) The momentum transfer cross section (in units of πa_0^2) as a function of momentum (in units of a_0^{-1}) for low-energy electron-He scattering. The MBPT-SDpT and KV cross sections are almost indistinguishable at the scale at which the graph is drawn.

section is that of the Australian National University (ANU) group [32] and was obtained by analyzing drift velocity measurements. The present momentum transfer cross section shown in Fig. 2 is barely different from the KV and the ANU σ_{MT} . At the lowest energies, the SDpT cross section is about 1%–2% larger than the ANU and KV σ_{MT} .

The SDpT momentum transfer cross section was used as input into a program to solve the Boltzmann equation in the two-term approximation and subsequently to compute the drift velocities for an electron swarm in helium gas. The drift velocities were then compared with the 77 K values from the ANU group [32]. The root-mean-square difference for values of E/N (the electric field to atom density ratio) ranging from 0.008 Townsend (Td) to 1.70 Td was 1.0% with a maximum discrepancy at any single E/N value not exceeding 2.0%. All of the discrepancies exceeding 1.0% occurred for

TABLE II. The MBPT-SDpT phase shifts (in units of rad) and cross sections (in units of πa_0^2) for e^- -He scattering. Phase shifts from a Kohn variational (KV) calculation [22] and the phase shifts for d -wave scattering calculated with MERT formula are also listed. The first row for the δ_0 column gives the scattering length (in units of a_0).

k	δ_0		δ_1			δ_2		σ_T	σ_{MT}
	SDpT	KV	SDpT	KV	MERT	SDpT	MERT		
0.00	1.189	1.1835						5.6549	5.6549
0.05	-0.062 45	-0.062 07	0.000 727	0.000 746	0.000 724	0.000 100	0.000 104	6.2350	6.3792
0.10	-0.1286	-0.1282	0.002 96	0.003 08	0.002 90	0.000 40	0.000 414	6.5882	6.8867
0.20	-0.2657	-0.2655	0.012 47	0.013 11	0.011 59	0.001 59	0.001 66	6.9425	7.5613
0.30	-0.4037	-0.4021	0.029 29	0.030 63	0.026 08	0.003 55	0.003 73	6.9797	7.8834
0.40	-0.5387	-0.5388	0.053 51	0.055 19	0.046 34	0.006 32	0.006 62	6.8093	7.9032
0.50	-0.6684	-0.6684	0.084 22	0.086 05	0.072 32	0.009 93	0.010 35	6.5077	7.6555
0.60	-0.7913	-0.7930	0.1196	0.1209	0.1040	0.014 41	0.014 90	6.1279	7.1839
0.70	-0.9064	-0.9067	0.1572	0.1588	0.1411	0.019 79	0.020 28	5.7043	6.5486
0.80	-1.0133	-1.0155	0.1947	0.1960	0.1834	0.026 06	0.026 49	5.2603	5.8212
0.90	-1.1117	-1.1163	0.2300	0.2305	0.2306	0.03319	0.033 52	4.8124	5.0694
1.00	-1.2015	-1.2056	0.2620	0.2626	0.2821	0.04115	0.041 38	4.3752	4.3482
1.10	-1.2817	-1.2848	0.2903	0.2932	0.3373	0.04992	0.050 05	3.9604	3.6929

TABLE III. Various estimates of the scattering length, A_{scat} (in units of a_0) for e^- -He scattering. A MERT analysis to extrapolate from finite energies was common to all experimental estimates of the phase shifts.

	A_{scat} (units of a_0)
HF	1.4825
DF	1.4824
MBPT-SD	1.184
MBPT-SD _{final}	1.187
MBPT-SDpT	1.189
KV [22]	1.1835
MCHF [26]	1.1784
R-matrix [25]	1.189
Polarized orbital [35]	1.1575
Expt. (Time of flight, ANU) σ_T [29]	1.16
Expt. (Drift velocity, ANU) σ_{MT} [32]	1.18(2)
Expt. (Angular distribution, Kaiserslautern) [36]	1.172
Expt. (Time of flight, Bielefeld) σ_T [31]	1.195

$E/N < 0.05$ Td where the mean energy of the swarm was smaller than 0.038 eV.

Scattering lengths from various sources are listed in Table III. Almost all of these values used a MERT analysis to estimate the scattering length from data at finite energies. The one exception was the MCHF calculation which was an explicit calculation at zero energy [26]. The most accurate experimental scattering lengths are expected to be those obtained by the analysis of swarm experiments that measure the drift velocity. Such experiments involve electron swarms at mean electron energies [32,33] lower than those of any other experiment. The value attributed to the drift velocity experiment in Table III, namely, 1.18(2) a_0 was taken from a fit of a MERT expansion to the momentum transfer cross section for energies below 0.20 eV [32]. The present SDpT scattering length was 1.189 a_0 and we have already noted that it is slightly larger than the experimental σ_{MT} at the lowest energies. The unimportance of relativistic effects for this system is demonstrated by the very small difference between the scattering lengths obtained in the DF and Hartree-Fock (HF) approximations.

An estimate of the overall uncertainty can be deduced from the $k = 0.20$ a_0^{-1} s -wave phase shift of -0.2650 rad obtained from the confined variational method [37]. This phase shift is 0.0005 rad larger than the KV phase shift and 0.000 65 rad larger than the MBPT-SDpT phase shift. It was taken from a variational calculation with correlated basis functions and is the most accurate phase so far obtained from an e^- -helium system.

Calculations of the total elastic cross section σ_T are compared with experimental measurements in Fig. 3. There have been many experimental investigations of the low-energy helium cross section and we have been selective about which measurements to depict. At low energies, determination of the electron energy is best done by the time of flight technique (TOF) so cross sections from the ANU [29] and Bielefeld [31] groups are shown. The transmission experiment of the Indiana group [30] is also plotted in Fig. 3. There is a tendency for the experimental cross sections to be too small by a few percent

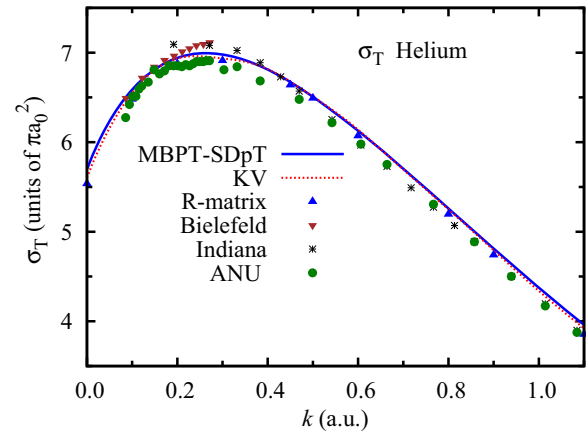


FIG. 3. (Color online) The elastic cross section (in units of πa_0^2) as a function of momentum (in units of a_0^{-1}) for low-energy electron-He scattering. The MBPT-SDpT and KV cross sections are almost indistinguishable at the scale at which the graph is drawn.

for $k > 0.40$ a_0^{-1} . However, the experimental uncertainties associated with these measurements are typically between 2% and 5%, and there is effectively no discrepancy between theory and experiment once these uncertainties are taken into consideration.

To summarize, the MBPT-SDpT cross sections are consistent at a 1%–2% level of agreement with the high-accuracy KV calculations and with the most accurate experimental elastic and momentum transfer sections.

IV. NEON

This electron-neon system is an 11-electron system that can be expected to be influenced by many-body effects. There have been a number of calculations [38,41,51–53] and experiments [31,40,47,49,50,54,55]. The MCHF calculation was a completely *ab initio* calculation focused on describing low-energy elastic scattering [38,53]. The B-spline R-matrix (BSR) calculation [41,42] was also *ab initio* and used a very large channel space, but was not optimized to describe low-energy scattering. The polarized orbital calculation used an *ab initio* polarization potential which was scaled so that it was consistent with the correct dipole polarizability at long distances from the nucleus [44,52].

The radius of the cavity was 48.0 a_0 . The lowest momentum for any of the box states was approximately 0.066 a_0^{-1} . Phase shifts were explicitly calculated for the s , $p_{1/2,3/2}$, and $d_{3/2,5/2}$ partial waves. The phase shifts for $\ell \geq 3$ were computed using Eq. (12). Spin-orbit splitting of the phase shifts was generally small; at $k = 0.7$ a_0^{-1} it was 1.5% for the p wave and 0.15% for the d wave.

Table IV reports estimates of the scattering lengths resulting from various calculations and experiments. The difference between a relativistic and a nonrelativistic calculation of the scattering length in the DF and HF approximations was only 0.001 a_0 . The inclusion of projectile-target correlations significantly reduced the scattering length. The positive scattering length indicates an s -wave interaction that is repulsive. The most accurate estimate of the scattering length, 0.214(5) a_0 , is

TABLE IV. The scattering length (in units of a_0) for e^- -Ne scattering. Apart from a few exceptions [38,39], the scattering lengths used a MERT analysis to convert finite-energy data to zero energy.

	A_{scat} (units of a_0)
HF	1.0641
DF	1.0630
MBPT-SD	0.252
MBPT-SD _{extra}	0.251
MBPT-SDpT	0.224
MCHF [38]	0.2218
Model potential fit to expt. σ_{MT} [39]	0.249
Phase shift analysis [43]	0.22
Polarized orbital [44]	0.201
Expt. (conductivity ratio, Sashkatchewan) σ_{MT} [45]	0.20
Expt. (drift velocity, ANU) σ_{MT} [40]	0.24
Expt. (microwave absorptivity, Paris) σ_{MT} [46]	0.24
Expt. (beam attenuation, Lockheed) σ_{T} [47]	0.30
Expt. (drift velocity, ANU) σ_{MT} [48]	0.214(5)
Expt. (time of flight, ANU) σ_{T} [49]	0.212
Expt. (time of flight, Bielefeld) σ_{T} [50]	0.217(6)

that deduced [48] from the drift velocity data of the ANU group [40]. MERT analyses of elastic cross-section data obtained from the time of flight method, namely, $0.212 a_0$ [49] and $0.217 a_0$ [34,44,50], are compatible with this drift velocity estimate. The MBPT-SDpT scattering length of $0.224 a_0$ lies within $0.01 a_0$ of these estimates and is about $0.002 a_0$ larger than the MCHF scattering length. No scattering length was reported for the BSR calculation.

Phases shifts and the elastic and momentum transfer cross sections are listed in Table V. The phase shifts are tabulated on a denser momentum grid in the Supplemental Material [34]. The largest momentum for which data are given is at $k = 0.86 a_0^{-1}$ as this is just below the energy for which stable energies could be determined for the s wave. The MCHF s -wave phase shifts [38,53] are slightly less negative than the SDpT phase shifts.

TABLE V. The MBPT-SDpT phase shifts (in units of rad) and cross sections (in units of πa_0^2) for e^- -Ne scattering. Phase shifts from an MCHF calculation [38,53] are also listed. The first row for the δ_0 column gives the scattering length (in units of a_0).

k	δ_0		δ_1			δ_2				σ_{T}	σ_{MT}	
	Present	MCHF	$p_{\frac{1}{2}}$	$p_{\frac{3}{2}}$	MCHF	$d_{\frac{3}{2}}$	$d_{\frac{5}{2}}$	MCHF	MERT			
0	0.224	0.2218									0.201	0.201
0.05	-0.017 43		0.001 09	0.001 09		0.000 189	0.000 189		0.000 200		0.4924	0.5514
0.1	-0.044 69	-0.0448	0.003 27	0.003 26	0.0034	0.000 759	0.000 759	0.0008	0.000 799		0.8116	0.9215
0.2	-0.1187	-0.1175	0.005 65	0.005 52	0.0065	0.003 08	0.003 08	0.0030	0.003 20		1.424	1.538
0.3	-0.2096	-0.2086	-0.001 39	-0.001 73	0.0004	0.007 18	0.007 18	0.0070	0.007 19		1.955	1.905
0.4	-0.3101	-0.3082	-0.021 50	-0.022 17	-0.0177	0.013 49	0.013 50	0.0130	0.012 78		2.422	2.089
0.5	-0.4162	-0.4118	-0.054 24	-0.055 28	-0.0482	0.022 65	0.022 67	0.0215	0.019 97		2.854	2.201
0.6	-0.5247		-0.096 93	-0.098 36		0.035 33	0.035 37		0.028 75		3.254	2.310
0.7	-0.6337	-0.6259	-0.1464	-0.1482	-0.1358	0.052 10	0.052 18	0.0486	0.039 12		3.608	2.443
0.8	-0.7427	-0.7327	-0.1982	-0.2006	-0.1872	0.073 40	0.073 50	0.0683	0.5109		3.903	2.603
0.86	-0.7850		-0.2133	-0.2218		0.088 68	0.088 65		0.059 01		3.839	2.576

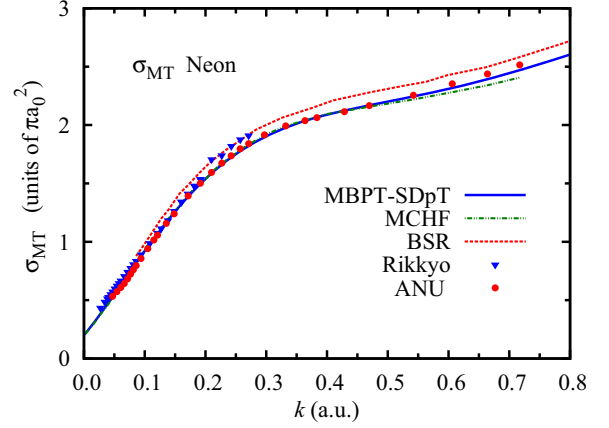


FIG. 4. (Color online) The momentum transfer cross section (in units of πa_0^2) as a function of momentum (in units of a_0^{-1}) for low-energy electron-Ne scattering.

Figure 4 shows the momentum transfer cross section. The presentation of data from other sources has been selective to avoid cluttering the graph. The ANU experimental σ_{MT} [40,48] was derived from drift velocity measurements that were accurate to better than 1%. The σ_{MT} from the University of Rikkyo was derived using drift velocity and characteristic energy measurements [55]. There are noticeable irregularities in the energy dependence of the Rikkyo σ_{MT} . The MCHF and BSR σ_{MT} are also depicted in Fig. 4. The MBPT-SDpT cross section is almost indistinguishable from the MCHF σ_{MT} over much of the momentum range shown in Fig. 4. Both MCHF and MBPT-SDpT cross sections are in close agreement with the experimental ANU σ_{MT} for almost all momenta. The only visible difference occurs for $k > 0.5 a_0^{-1}$, where the MCHF σ_{MT} is slightly smaller than the present and experimental σ_{MT} . The Rikkyo cross section is significantly larger than the ANU σ_{MT} over a couple of momentum ranges. The BSR calculation does not have the same level of agreement with the experimental ANU σ_{MT} . The MCHF calculation was specifically designed to address low-energy scattering while

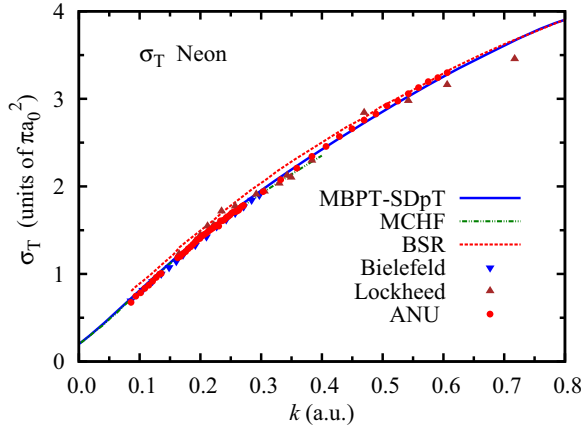


FIG. 5. (Color online) The elastic cross section (in units of πa_0^2) as a function of momentum (in units of a_0^{-1}) for low-energy electron-neon scattering. The MCHF and MBPT-SDpT cross sections are practically identical on the scale of the diagram. The cross sections attributed to the Bielefeld group have not been published by that group but they have previously been embedded in graphs comparing experimental cross sections with polarized orbital calculations [34,44,50].

the BSR calculation aimed to describe scattering over a much larger energy range.

The largest discrepancy between the MBPT-SDpT and ANU σ_{MT} [40] was only 4.5% and occurred at $k = 0.0717 a_0^{-1}$. However, a close examination of the ANU σ_{MT} revealed a slight dip in the shape of their σ_{MT} near this momentum that is most likely a consequence of the method used to construct the σ_{MT} , i.e., manual adjustment of individual cross-section values. A better test of the MBPT-SDpT σ_{MT} was to compute the drift velocities for an electron swarm in neon gas. The Boltzmann equation was solved using the two-term approximation. The drift velocities were then compared with the 77 K values from the ANU group [40]. The root-mean-square difference for values of E/N ranging from 0.002 to 1.70 Td was 1.2% with a maximum discrepancy at any single E/N value not exceeding 2.0%. All of the discrepancies exceeding 1.0% occurred for $E/N < 0.005$ Td where the mean energy of the swarm was smaller than 0.070 eV.

The elastic cross section is shown in Fig. 5. It is very difficult to distinguish between the MCHF and MBPT-SDpT σ_T cross sections. The MBPT-SDpT σ_T tracks the TOF cross sections very closely but is marginally larger ($\approx 5\%$ or less) for $k < 0.30 a_0^{-1}$. The experimental uncertainties for the TOF cross sections are typically 4%–5%. Data from the Bielefeld group [34,44,50] are only available for $k < 0.30 a_0^{-1}$, but are in almost perfect agreement with the ANU TOF experiment [49]. That the MBPT-SDpT cross section is marginally larger than the ANU and Bielefeld σ_T at the lowest momentum is consistent with the scattering lengths given in Table IV.

The overall summary for low-energy neon scattering is that there are two calculations, MBPT-SDpT and MCHF, and three experiments, the drift velocity at ANU and the TOF experiments at ANU and Bielefeld that give a set of cross sections that are generally consistent at a 1%–2% level of agreement once experimental uncertainties are taken into account.

TABLE VI. The scattering length (in units of a_0) for e^- -Kr scattering. Apart from a few exceptions [64,72], the scattering lengths were determined by a MERT analysis to an experimental or theoretical data set.

Method	A_{scat} (units of a_0)
HF	1.592
DF	1.500
MBPT-SD	−4.18
MBPT-SD _{extra}	−3.84
MBPT-SDpT	−3.23
BSR [42,72]	−3.72
Polarized orbital [71]	−3.10
Expt. (attenuation, KEK) σ_T [61]	−3.06(2)
Expt. (TOF, ANU) σ_T [21,62]	−3.28
Expt. (drift velocity, Westinghouse) σ_{MT} [75]	−3.32
Expt. (drift velocity, ANU) σ_{MT} [64,67]	−3.353
Expt. (drift velocity, ORNL) σ_{MT} [73]	−3.36(3)
Expt. (drift velocity, ANU) σ_{MT} [64]	−3.434
Expt. (angular distribution, Kaiserslautern) σ_T [57]	−3.478

V. KRYPTON

Krypton is an atom with 36 electrons and the electron collision dynamics will be influenced by direct and indirect relativistic effects. Direct effects include modifications to the scattering wave function due to relativistic effects resulting from the effective interaction between the target and scattering electrons. Indirect effects include a target wave function that is different due to relativistic effects. There have been a number of experimental determinations of the elastic cross section [34,50,56–62] and the momentum transfer cross section [63–67]. Of the many calculations of the electron-krypton system [56,68–72], the BSR calculation [42,72] is the most complete *ab initio* calculation. The BSR calculation was explicitly relativistic, being based on the Dirac equation. The BSR calculation employed a very large channel space, but was not optimized to describe low-energy scattering.

The cavity radius chosen for the MBPT calculations was $60.0 a_0$. The lowest-energy state for this atom was at a momentum of $k \approx 0.050 a_0^{-1}$.

Scattering lengths are presented in Table VI. Once again, an indication of the impact of a relativistic Hamiltonian can be gained from a comparison between the DF and HF scattering lengths. The difference was $0.10 a_0$. The polarization interaction leads to the effective electron-krypton interaction becoming significantly more attractive. The three different MBPT calculations gave values between -3.23 and $-4.18 a_0$, with the SDpT value being $-3.23 a_0$.

On the experimental side, scattering lengths have been estimated by MERT analysis of the total elastic and momentum transfer cross sections. There have been two analyses where MERT parameters were used to fit drift velocities for Kr-H₂ mixtures measured at ANU [66,67]. The most complete analysis using ANU data [67] gave $-3.353 a_0$ for the scattering length. An analysis of drift velocity measurements for pure Kr from Oak Ridge National Laboratory (ORNL) gave $-3.36(3) a_0$ [73]. The functional form of the MERT expressions used to extract the scattering length is important and expressions better

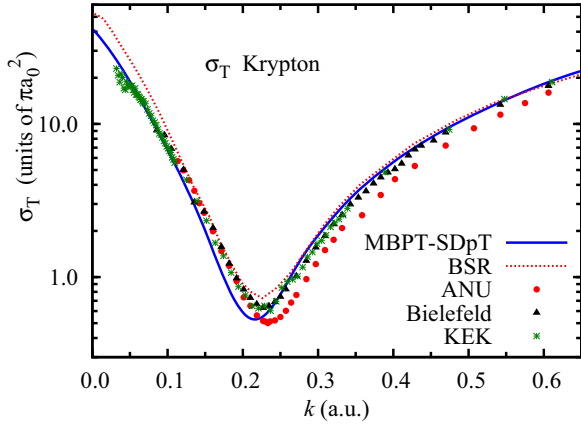


FIG. 6. (Color online) The elastic cross section (in units of πa_0^2) as a function of momentum (in units of a_0^{-1}) for low-energy electron-krypton scattering. The cross sections attributed to the Bielefeld group have not been published by that group but they have previously been embedded in graphs comparing experimental cross sections with polarized orbital calculations [34,50,56].

able to reproduce the behavior of short-range interactions are integral to performing the MERT analysis [21]. For example, the scattering length changed from $-3.19 a_0$ to $-3.28 a_0$ when the MERT expression for the p wave was modified to include two (rather than one) adjustable parameters in an analysis of the ANU σ_T [21,62]. The scattering length obtained from the phase shift analysis of low-energy Kr differential cross sections [57] used a MERT expression that was not accurate over the energy range over which it was applied [21]. A scattering length of $-3.06(2) a_0$ was obtained from the σ_T experiment at the High Energy Accelerator Research Organization located in Tsukuba, Japan (KEK) [61]. The KEK experiment produces electrons with energies as low as 14 meV by using a synchrotron to photoionize argon atoms. The scattering length from this experiment is smaller in magnitude than that of any other experiment and can be regarded as an outlier. It is worth noting that the electron-argon cross section has also been measured at KEK and the KEK scattering length was also lower in magnitude than most values derived from experiment [61].

The electron-krypton σ_T shown in Fig. 6 varies rapidly at the low energies below the deep Ramsauer-Townsend (RT) minimum. Besides the SDpT σ_T , cross sections from the BSR calculation [42,74] are also displayed. The BSR calculation is fully *ab initio* and used a very large channel space, but was not optimized to describe low-energy scattering.

The BSR calculation tends to overestimate the elastic cross section at energies below the RT minimum while the SDpT cross section tends to underestimate the elastic cross section at these energies. The shape of the KEK σ_T at the lowest energies is quite unusual. The KEK σ_T is in good agreement with the MBPT-SDpT σ_T for $k \in [0.05, 0.12] a_0^{-1}$ but falls below the MBPT-SDpT σ_T for $k < 0.05 a_0^{-1}$ and is larger than the MBPT-SDpT σ_T for $k \in [0.15, 0.22] a_0^{-1}$. The constraints imposed by effective range theory on the energy dependence of the low-energy phase shifts suggest that the KEK σ_T should be treated with caution.

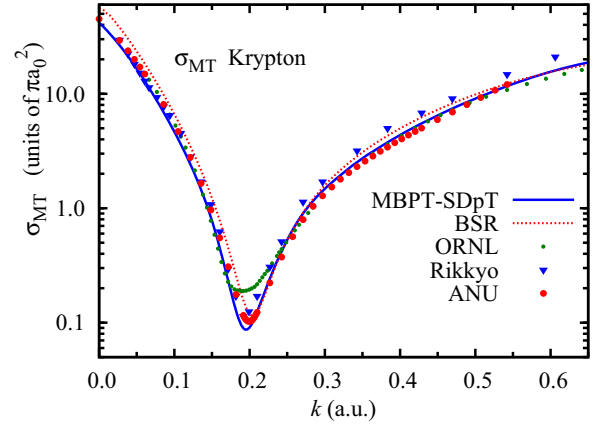


FIG. 7. (Color online) The momentum transfer cross section (in units of πa_0^2) as a function of momentum (in units of a_0^{-1}) for low-energy electron-krypton scattering.

The SDpT calculation gives the Ramsauer minimum at an energy lower than that of any of the cross sections shown in Fig. 6. This is consistent with the SDpT calculation having a scattering length that is smaller in magnitude. There is a tendency for differences between the BSR and SDpT σ_T to vanish at energies above the Ramsauer minimum. This cancellation of differences was also apparent in comparisons of the SDpT, SD, and SD_{extra} σ_T cross sections. At $k = 0.5 a_0^{-1}$, the elastic cross sections are 11.06, 11.16, and $10.93 \pi a_0^2$, respectively, a variation of only 2%. The variation amongst these cross sections at the $E = 0$ threshold is about 40%.

Comparisons with the momentum transfer cross section in Fig. 7 show that the SDpT σ_{MT} tends to underestimate the experimental data from the ANU group [67] while the BSR σ_{MT} tends to overestimate the experimental data at energies below the RT minimum. However, the BSR and SDpT σ_{MT} tend to be in close agreement at energies above the RT minimum. The BSR and SDpT σ_{MT} are also in close agreement with the experimental values from the ANU and ORNL groups above the RT minimum.

Phase shifts for the individual partial waves are tabulated in Table VII. The s -wave and p -wave phase shifts both go through zero for momentum between 0.2 and $0.3 a_0^{-1}$, and this contributes to the depth of the Ramsauer minimum. The phase shifts are tabulated on a denser momentum grid in the Supplemental Material [34].

Our overall summation for krypton is that the SDpT calculation tends to underestimate the scattering length by about 4%. The 25% differences between the SD, SD_{extra} , and SDpT scattering lengths indicate that triple excitations have a significant impact on the scattering length. Comparisons with the BSR cross sections and experimental cross sections suggest a high degree of consistency for energies from 1 to 7 eV, with the outlier being the ANU TOF cross sections that are about 25% smaller than most other cross sections.

VI. PERSPECTIVES AND CONCLUSIONS

The low-energy phase shifts for electron scattering from helium, neon, and krypton have been computed with the all-order single-double implementation of relativistic many-body

TABLE VII. The MBPT-SDpT phase shifts (in units of rad) and cross sections (in units of πa_0^2) for e^- -Kr scattering. The first row for the δ_0 column gives the scattering length (in units of a_0).

k	δ_0	δ_1		δ_2		δ_3		MERT	σ_T	σ_{MT}
	s	$p_{\frac{1}{2}}$	$p_{\frac{3}{2}}$	$d_{\frac{3}{2}}$	$d_{\frac{5}{2}}$	$f_{\frac{5}{2}}$	$f_{\frac{7}{2}}$			
0	-3.23								41.73	41.73
0.05	0.1082	0.067 23	0.066 15	0.001 20	0.001 20	0.000 390	0.000 390	0.000 418	18.90	16.55
0.1	0.1251	0.019 91	0.019 06	0.004 73	0.004 73	0.001 56	0.001 56	0.001 67	6.743	4.643
0.2	0.019 93	0.032 96	0.027 56	0.020 24	0.020 29	0.006 25	0.006 25	0.006 69	0.5898	0.0931
0.3	-0.1548	-0.027 65	-0.015 65	0.052 13	0.052 45	0.014 22	0.014 22	0.015 05	1.877	1.481
0.4	-0.3500	-0.086 58	-0.1073	0.1124	0.1135	0.025 82	0.025 84	0.026 75	5.635	4.371
0.5	-0.5501	-0.2012	-0.2290	0.2196	0.2220	0.041 84	0.041 91	0.041 80	11.06	9.081
0.6	-0.7503	-0.3321	-0.3655	0.3936	0.3972	0.063 69	0.063 87	0.060 20	18.27	15.58
0.64	-0.8272	-0.3816	-0.4176	0.4828	0.4863	0.074 46	0.074 67	0.068 49	21.43	18.17

perturbation theory. This represents the application of an approach to the description of atomic structure that has been very successful in describing single-electron atoms and ions. These phase shifts were computed without a single modification of the program that has been used to compute wave functions and expectation values for a number of atoms and ions [14]. The electron-atom scattering problem is more challenging, one reason being that the polarizabilities of the targets are all larger than the polarizabilities of corresponding isoelectronic alkali-metal ions. Consequently, correlation effects are stronger for the electron-atom scattering problem than for the corresponding electron-ion structure problem. However, the low-energy MBPT-SDpT cross sections are in good agreement with experiment. The scattering lengths for the electron-helium and electron-neon systems lie within 0.01 a_0 of the scattering lengths derived from the analysis of swarm experiments. The same level of agreement is not achieved for krypton, but here the difference from experiment is still only 4%. Previously, the most sophisticated *ab initio* calculation, the BSR calculation [42,72], gave a scattering length that was 10% larger than experiment.

Examination of the higher- ℓ phase shifts reveals some interesting features. At the lowest energies for the higher- ℓ partial waves, one expects calculated phase shifts to converge to the MERT formula. However, this does not occur. For helium, the SDpT d -wave phase shifts are slightly smaller than the MERT phase shifts. The same principle applies for d -wave phase shifts for $k \leq 0.3 a_0^{-1}$ for neon. A similar result occurs for the f -wave phase shifts for krypton. At $k = 0.3 a_0^{-1}$, the SDpT phase shift is 0.0142 rad while the MERT expression gives 0.0150 rad. These low-energy limitations in the higher- ℓ SDpT phase shifts do not have much impact on the cross sections. But they do indicate that a theoretical methodology that includes triple excitations perturbatively does not capture 100% of the electron-atom polarization interaction.

While the present approach is restricted to energies below the first ionization threshold, this is possibly the most interesting energy region since the electron-atom cross section is most sensitive to the fine details of the electron-atom interaction at these energies. The scattering length of course is a very useful parameter with which to characterise the electron-atom interaction. The extension of the method to other rare gas systems, such as Ar, Xe, and Rn would be straightforward. The very-low-energy scattering of electrons from the alkali metals in the energy region between the ns and np thresholds would also be straightforward using the recently developed configuration interaction plus MBPT or configuration interaction plus all-order methods [76–78]. Application to energy regions where inelastic events are possible would need modifications of the underlying atomic structure program.

The present calculations to some extent sit outside the mainstream of the most recent electron scattering research. There has been more activity in developing theories that do a reasonable job of modeling excitation and ionization cross sections over a large energy range. The emphasis had been more on describing the excitations (including ionization) than purely elastic scattering. However, the very-low-energy region is the energy region that is the most sensitive to the fine details of the electron-atom interaction. An interesting challenge for the future will be the development of a fully *ab initio* computational procedure that is demonstrably converged with respect to numerical (e.g., basis set) aspects and is capable of predicting the scattering lengths for the rare gases to a precision of 1%.

ACKNOWLEDGMENTS

This work was partially supported under the Australian Research Council's (ARC) Centre of Excellence program. The work of M.S.S. was supported in part by National Science Foundation Grant No. PHY-1068699.

- [1] V. Risberg, Arch. Math. Naturvidenskab **53**, 1 (1956).
- [2] I. C. Percival, Proc. Phys. Soc. A **70**, 494 (1957).
- [3] Y. Alhassid and S. E. Koonin, Ann. Phys. **155**, 108 (1984).
- [4] J. Shumway and D. M. Ceperley, Phys. Rev. B **63**, 165209 (2001).

- [5] S. Chiesa, M. Mella, and G. Morosi, Phys. Rev. A **66**, 042502 (2002).
- [6] M. van Faassen, A. Wasserman, E. Engel, F. Zhang, and K. Burke, Phys. Rev. Lett. **99**, 043005 (2007).
- [7] K. M. Nollert, S. C. Pieper, R. B. Wiringa, J. Carlson, and G. M. Hale, Phys. Rev. Lett. **99**, 022502 (2007).

- [8] G. F. Gribakin and J. Ludlow, *Phys. Rev. A* **70**, 032720 (2004).
- [9] W. R. Johnson, S. A. Blundell, and J. Sapirstein, *Phys. Rev. A* **37**, 307 (1988).
- [10] J. Sapirstein and W. R. Johnson, *J. Phys. B* **29**, 5213 (1996).
- [11] H. Bachau, E. Cormier, P. Decleva, J. E. Hansen, and F. Martín, *Rep. Prog. Phys.* **64**, 1815 (2001).
- [12] I. P. Grant, *J. Phys. B* **42**, 055002 (2009).
- [13] M. S. Safronova, A. Derevianko, and W. R. Johnson, *Phys. Rev. A* **58**, 1016 (1998).
- [14] M. S. Safronova and W. R. Johnson, *Adv. At. Mol. Opt. Phys.* **55**, 191 (2008).
- [15] A. Chodos, R. L. Jaffe, K. Johnson, C. B. Thorn, and V. F. Weisskopf, *Phys. Rev. D* **9**, 3471 (1974).
- [16] M. E. Rose, *Relativistic Electron Theory* (Wiley, New York, 1961).
- [17] J. Mitroy, M. S. Safronova, and C. W. Clark, *J. Phys. B* **43**, 202001 (2010).
- [18] M. S. Safronova, W. R. Johnson, and A. Derevianko, *Phys. Rev. A* **60**, 4476 (1999).
- [19] T. F. O'Malley, *Phys. Rev.* **125**, 1300 (1962).
- [20] T. F. O'Malley, *Phys. Rev.* **130**, 1020 (1963).
- [21] S. J. Buckman and J. Mitroy, *J. Phys. B* **22**, 1365 (1989).
- [22] R. K. Nesbet, *Phys. Rev. A* **20**, 58 (1979).
- [23] R. K. Nesbet, *J. Phys. B* **12**, L243 (1979).
- [24] R. P. McEachran and A. D. Stauffer, *Aust. J. Phys.* **50**, 511 (1997).
- [25] T. F. O'Malley, P. G. Burke, and K. A. Berrington, *J. Phys. B* **12**, 953 (1979).
- [26] H. P. Saha, *Phys. Rev. A* **48**, 1163 (1993).
- [27] S. J. Buckman and M. J. Brunger, *Aust. J. Phys.* **50**, 483 (1997).
- [28] S. J. Buckman and J. P. Sullivan, *Nucl. Instrum. Methods Phys. Res., Sect. B* **247**, 5 (2006).
- [29] S. J. Buckman and B. Lohmann, *J. Phys. B* **19**, 2547 (1986).
- [30] R. E. Kennerly and R. A. Bonham, *Phys. Rev. A* **17**, 1844 (1978).
- [31] W. Ferch, J. Raith, and K. Schroder, *J. Phys. B* **13**, 1481 (1980).
- [32] R. W. Crompton, M. T. Elford, and A. G. Robertson, *Aust. J. Phys.* **23**, 667 (1970).
- [33] R. W. Crompton, M. T. Elford, and R. L. Jory, *Aust. J. Phys.* **20**, 369 (1967).
- [34] See Supplemental Material at <http://link.aps.org/supplemental/10.1103/PhysRevA.89.012701> for tables of MBPT-SDpT phase shifts and cross sections in more detail. The unpublished cross sections for Ne and Kr from the University of Bielefeld group are also tabulated.
- [35] R. P. McEachran and A. D. Stauffer, *J. Phys. B* **16**, 255 (1983).
- [36] D. Andrick and A. Bitsch, *J. Phys. B* **8**, 402 (1975).
- [37] J. Y. Zhang, J. Mitroy, and K. Varga, *Phys. Rev. A* **78**, 042705 (2008).
- [38] H. P. Saha, *Phys. Rev. Lett.* **65**, 2003 (1990).
- [39] C. Bottcher, *J. Phys. B* **4**, 1140 (1971).
- [40] A. G. Robertson, *J. Phys. B* **5**, 648 (1972).
- [41] O. Zatsarinny and K. Bartschat, *Phys. Rev. A* **85**, 062710 (2012).
- [42] O. Zatsarinny and K. Bartschat, *Electron Scattering Database* (2012), <http://www.lxcat.laplace.univ-tlse.fr>.
- [43] M. R. C. McDowell, *J. Phys. B* **4**, 1649 (1971).
- [44] R. P. McEachran and A. D. Stauffer, *Phys. Lett. A* **107**, 397 (1985).
- [45] C. R. Hoffmann and H. M. Skarsgard, *Phys. Rev.* **178**, 168 (1969).
- [46] C. Sol, F. Devos, and J.-C. Gauthier, *Phys. Rev. A* **12**, 502 (1975).
- [47] A. Salop and H. H. Nakano, *Phys. Rev. A* **2**, 127 (1970).
- [48] T. F. O'Malley and R. W. Crompton, *J. Phys. B* **13**, 3451 (1980).
- [49] R. J. Gulley, D. T. Alle, M. J. Brennan, M. J. Brunger, and S. J. Buckman, *J. Phys. B* **27**, 2593 (1994).
- [50] J. Ferch and W. Raith, unpublished cross section data from the Bielefeld group, 1985.
- [51] W. C. Fon and K. A. Berrington, *J. Phys. B* **14**, 323 (1981).
- [52] R. P. McEachran and A. D. Stauffer, *J. Phys. B* **16**, 4023 (1983).
- [53] H. P. Saha, *Phys. Rev. A* **39**, 5048 (1989).
- [54] I. Linert, B. Mielewska, G. C. King, and M. Zubek, *Phys. Rev. A* **74**, 042701 (2006).
- [55] T. Koizumi, H. Murakoshi, S. Yamamoto, and I. Ogawa, *J. Phys. B* **17**, 4387 (1984).
- [56] D. J. R. Mimmagh, R. P. McEachran, and A. D. Stauffer, *J. Phys. B* **26**, 1727 (1993).
- [57] M. Weyhreter, B. Barzick, A. Mann, and F. Linder, *Z. Phys. D* **7**, 333 (1988).
- [58] I. Linert, B. Mielewska, G. C. King, and M. Zubek, *Phys. Rev. A* **81**, 012706 (2010).
- [59] M. Kurokawa, M. Kitajima, K. Toyoshima, T. Odagiri, H. Kato, H. Kawahara, M. Hoshino, H. Tanaka, and K. Ito, *Phys. Rev. A* **82**, 062707 (2010).
- [60] M. Kitajima, M. Kurokawa, T. Kishino, K. Toyoshima, T. Odagiri, H. Kato, K. Anzai, M. Hoshino, H. Tanaka, and K. Ito, *Eur. Phys. J. D* **66**, 130 (2012).
- [61] M. Kurokawa, M. Kitajima, K. Toyoshima, T. Kishino, T. Odagiri, H. Kato, M. Hoshino, H. Tanaka, and K. Ito, *Phys. Rev. A* **84**, 062717 (2011).
- [62] S. J. Buckman and B. Lohmann, *J. Phys. B* **20**, 5807 (1987).
- [63] T. Koizumi, E. Shirakawa, and I. Ogawa, *J. Phys. B* **19**, 2331 (1986).
- [64] J. P. England and M. T. Elford, *Aust. J. Phys.* **41**, 701 (1988).
- [65] M. Suzuki, T. Taniguchi, and H. Tagashira, *J. Phys. D* **22**, 1848 (1989).
- [66] J. Mitroy, *Aust. J. Phys.* **43**, 19 (1990).
- [67] M. J. Brennan and K. F. Ness, *Aust. J. Phys.* **46**, 249 (1993).
- [68] K. L. Bell, K. A. Berrington, and A. Hibbert, *J. Phys. B* **21**, 4205 (1988).
- [69] J. Yuan and Z. Zhang, *J. Phys. B* **22**, 2581 (1989).
- [70] K. L. Baluja, A. Jain, H. W. Jones, C. A. Weatherford, and A. Amaya-Tapia, *Phys. Scr.* **45**, 30 (1992).
- [71] R. P. McEachran and A. D. Stauffer, *J. Phys. B* **17**, 2507 (1984).
- [72] O. Zatsarinny, K. Bartschat, and M. Allan, *Phys. Rev. A* **83**, 032713 (2011).
- [73] S. R. Hunter, J. G. Carter, and L. G. Christophorou, *Phys. Rev. A* **38**, 5539 (1988).
- [74] O. Zatsarinny, K. Bartschat, and M. Allan, *J. Phys.: Conf. Ser.* **388**, 012008 (2012).
- [75] L. S. Frost and A. V. Phelps, *Phys. Rev.* **136**, A1538 (1964).
- [76] S. G. Porsev and A. Derevianko, *J. Exp. Theor. Phys.* **102**, 195 (2006).
- [77] M. S. Safronova, M. G. Kozlov, and C. W. Clark, *Phys. Rev. Lett.* **107**, 143006 (2011).
- [78] M. S. Safronova, S. G. Porsev, M. G. Kozlov, and C. W. Clark, *Phys. Rev. A* **85**, 052506 (2012).